Gravitational Aggregates: Evidence and Evolution

D. C. Richardson
University of Maryland at College Park

Z. M. Leinhardt
University of Maryland at College Park

H. J. Melosh
University of Arizona

W. F. Bottke Jr.
Southwest Research Institute at Boulder

E. Asphaug
University of California at Santa Cruz

It has been suggested that asteroids between ~100 m and ~100 km in size may be gravitational aggregates of loosely consolidated material. Recently evidence has been mounting to support this idea. Comet breakups, crater chains, doublet craters, giant craters, grooves, asteroid spins, underdense asteroids, asteroid satellites, and unusual asteroid shapes can all be explained to some degree by the properties of aggregate structures. Moreover, laboratory and numerical experiments indicate that solid asteroids, if they existed, would likely be completely shattered by now, owing to their violent collisional histories. Once shattered, a body becomes increasingly difficult to disrupt since it can efficiently absorb energy deposited at the impact site. In this chapter we present the evidence for gravitational aggregates and discuss the implications of their existence for asteroid evolution. We also propose a new classification scheme for asteroid structure parameterized by fundamental quantities such as strength and porosity.

1. DEFINITIONS

Over 50 years ago, *Jeffreys* (1947) and *Öpik* (1950) introduced the idea that some asteroids and comets (collectively, planetesimals) may not be solid objects governed solely by material strength. While investigating the distortion and disruption effects of planetary tides, both came to the conclusion that tidal forces in the solar system could not significantly affect solid objects. Nearly three decades later, *Chapman* (1978) used the term "rubble pile" to describe a gravitationally bound collection of boulders, arguing that high-speed collisions between main-belt asteroids would cause extensive fracturing and erosion, turning such asteroids into rubble. Later, *Weissman* (1986) suggested comets may be "primordial rubble piles" in order to explain the comparatively high frequency of comet-splitting events. Currently, "rubble pile" is used in the planetary science community to describe a variety of configurations that range from theoretical constructs like piles of marbles to more realistic speculations on planetesimal interiors, and some confusion has arisen as to precise definitions.

In an effort to standardize terms, we propose a new scheme for describing the range of possible asteroid (and, to a certain extent, comet) configurations. We have selected parameters that convey a sense of how a given planetesimal will react to the most important geological processes affecting such bodies today, namely short-term stresses like collisions (and possibly manmade explosions), and long-term stresses such as tidal forces and rotational spinup. (Here "short" and "long" refer to the interval over which the load is applied divided by the time it takes a seismic wave to travel the diameter of the object.) The definitions also provide some idea of the origin or collisional history of the object. It is important to emphasize that the classification is meant as a bridge between theory and observation, not a tool for mapping observed asteroids. Some parameters may be directly measurable (from ground or flyby observation, or even from *in situ* seismic mapping in the future) but others perhaps can only be inferred from theory. The aim is to provide a useful starting point from which both observers and theorists can make firm predictions.

In the proposed scheme, the term "rubble pile" becomes more specific, referring to a particular class of broken-up objects. We assign, at a minimum, two parameters that uniquely locate the object on a diagram that ranges from zero consolidation (rubble pile) to perfect consolidation (monolith). In addition, we augment the classification by the size of the object's largest component, if applicable, and treat regolith, contact binaries, and other such compound structures as special cases. We omit differentiated objects (such as Vesta)

entirely. The classification is not exhaustive, nor is it meant to be: The hope is that future study will add detail to this simple scheme, without sacrificing the fundamentals.

The two principal parameters in our classification scheme are porosity

$$\text{porosity} = 1 - \frac{\text{sum of component volumes}}{\text{bulk volume}} = \frac{\text{sum of void space}}{\text{bulk volume}} \quad (1)$$

and relative tensile strength

$$\text{RTS} = \frac{\text{tensile strength of object}}{\text{mean tensile strength of components}} \quad (2)$$

where "tensile strength" is the maximum stress (force per unit area) — applied in a way that tends to cause separation across the plane on which it acts — that a body can withstand before fracture or rupture occurs. These parameters are dimensionless and vary from 0 to 1, both desirable properties. We are deliberately vague in our notion of "component" since the aim is to measure and compare bulk quantities, not detailed internal properties, although evidently some assumption as to the nature of the components is present in the definition of RTS. Similarly, we do not distinguish between micro- and macroporosity, since a macroporous asteroid (with voids between components) could be made up of microporous components (with voids inside the components), adding an undesirable level of complication. Such a distinction, however, may be important for understanding detailed collisional physics: Both configurations damp impact energy, but in a different way, the former via excavation and ejection, the latter through compaction and crushing (cf. sections 2.2 and 2.3). These details are beyond the scope of our simple classification but can always be added later. Finally, we recognize that various factors can contribute to overall strength, including shear strength (the internal resistance of a body to tangential stress, which typically includes a frictional component) and even geometrical locking between pieces, but again for our purposes we choose not to distinguish between these cases. Instead, using just porosity and RTS as defined, we can roughly predict how asteroids and comets will react to the primary geological processes affecting these bodies today, which is our primary goal.

To these parameters we adopt a secondary measure proposed by *Campo Bagatin and Petit* (2001), the mass fraction of the largest component

$$\text{MF} = \frac{\text{mass of largest component}}{\text{total mass of object}} \quad (3)$$

With this definition we can state that bodies with $\text{MF} \geq 0.5$ are more properly termed compound objects, such as regolith overlying a large consolidated component, or a contact binary with one lobe thoroughly damaged. Detail regarding the size distribution of the components can always be added, such as a single power-law exponent (if appropriate), or even a ratio of higher-order moments of the size distribution (e.g., sum of component volumes divided by sum of component surface areas, normalized by the mean diameter of the object). This level of detail may be more appropriate for theorists discussing a numerical model (e.g., monodispersive vs. size distribution) or for observers who have achieved a comprehensive characterization of the particle sizes in the surface layer of the object in question, for example. It may be better in some cases to simply distinguish between "fine" and "coarse" particles.

Figure 1 shows two realizations of the RTS vs. porosity parameter space in this scheme, with the plot on the left showing proposed structural classifications for distinct regions and the plot on the right showing how objects in these regions will react to stress. We deliberately omit quantitative values or sharp divisions, since many details regarding these structures are unknown at this time. In simple terms, objects with low RTS are more susceptible to tidal disruption than objects with high RTS, and objects with low porosity are less efficient at absorbing impact energy than objects with high porosity. We elaborate on these points in the following brief qualitative descriptions of the regions.

Monolithic (bottom right): These objects are essentially unaffected by long-term stresses like planetary tidal forces. For highly energetic events such as collisions or explosions, the compressive wave easily reaches the farside of the object, reflecting as a tensive wave that can produce damage and spalls.

Fractured (bottom middle): These objects may have a significant number of faults and/or joints and may lack enough tensile strength to resist disruption by long-term stresses. Our definition implies that the original structure of the object is still largely in place (hence the low porosity). However, the definition is open to more complicated histories, for example, a previously reassembled object may have been tamped down into a less-porous structure, resembling a simple fractured body.

Shattered (bottom left): These objects are related to fractured bodies, except that they are even more susceptible to disruption from long-term stresses like tidal forces or rotational spinup. A body in this category could be characterized as an object cleaved into a few large components or one whose structure is dominated by joints and cracks. Like the fractured body, the original structure of the object is mostly in place. The RTS of a shattered object may be larger than zero, since jagged or interlocking edges and friction may allow the object to resist some stresses. The reaction of this body to short-term stresses like collisions is different from a simple monolith. Spalls are damped and the tensile wave is suppressed, such that this object is more difficult to disrupt. Small craters formed on single components of the body may act like they were formed on a monolith.

Shattered with rotated components (lower middle): An object in this category has had its original pieces displaced

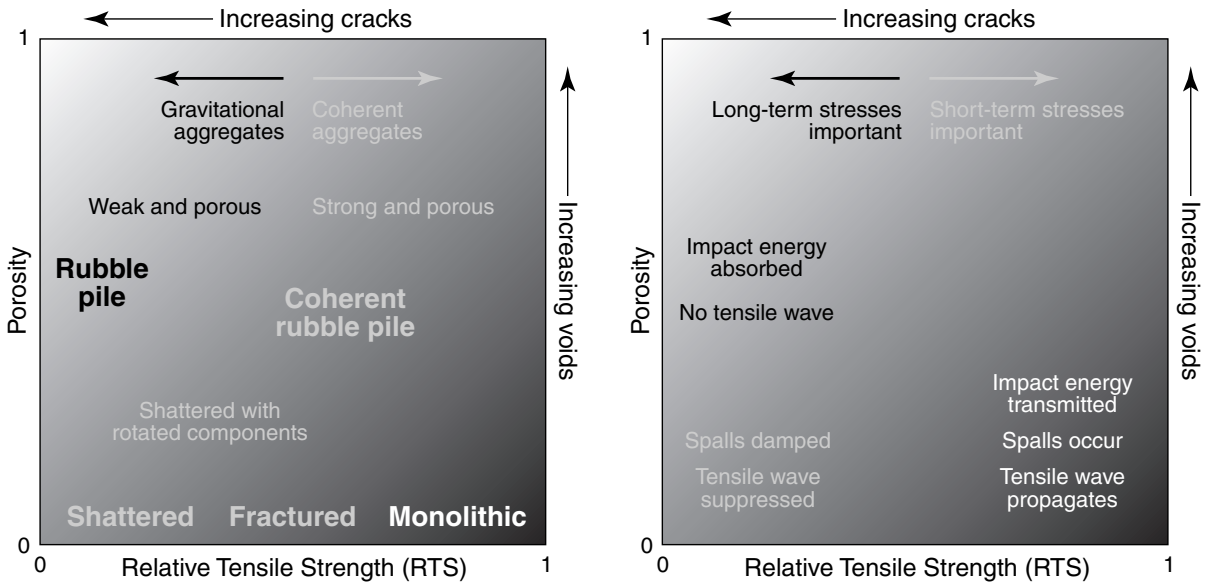

Fig. 1. The RTS-porosity parameter space. The plot on the left assigns labels to distinct regions on the basis of internal structure. The plot on the right describes how objects correspondingly react to stress in these regions. The divisions are deliberately vague and qualitative since the quantitative details are poorly known.

and reoriented somewhat, although much of the original structure may remain. It may contain void spaces, or possibly some cracks may be filled with regolith, although these features do not dominate its overall structure.

Rubble pile (middle left): This structure is literally a pile of rubble, with the organization that you might expect from a bunch of rocks dumped from a truck. A body that has been completely shattered and reassembled may fit into this category. The "bowling-ball," "marble," or "sand" piles used in numerical models (as simplified constructs of real rubble piles) also fit in this category. Typically a real rubble pile has moderate porosity because of the disorganization, but note that the porosity of a group of equal-size spheres can range from 0.26 (hexagonal or cubic closest packing) to 0.48 (simple cubic packing), and yet both configurations are highly ordered.

We deliberately omit any notion of particle size from this definition. Formally, "rubble" is breccia (angular rock fragments) without any cement or glue, distinguished from a shattered body by its rotated components (*Jackson,* 1997). A researcher may have a certain notion for the fragment sizes in this context, though it is not a formal part of the definition. Instead, it is more appropriate to qualify the sizes as needed, using formal definitions of particle types (i.e., silt, sand, pebble, boulder) if desired. With this in mind, for our classification, "rubble" can be anything from tiny grains of clay to boulders tens of kilometers across or even larger, unless specified otherwise.

The reaction of rubble piles to short-term stresses like collisions is absorption of impact energy via compression, with little to no tensile wave developed in the structure. Thus, impact energy is muffled and often goes into heat. Conversely, long-term tidal stresses can completely pull a rubble pile apart.

Coherent rubble pile (middle): This group is for rubble piles whose components have somehow become attached or cemented to one another. This would give the objects some RTS.

Weak and porous/strong and porous (top): These objects have low to high tensile strength with high porosity, something akin to dust bunnies, pumice, or aerogel. Comet nuclei are often described as weak and porous (e.g., *Bockelée-Morvan et al.,* 2001).

What is missing so far in this categorization is an overall term that describes bodies made up of multiple components, i.e., bodies that are not pure monoliths. We propose "aggregate" for this purpose, without being too specific about the detailed configuration. This can be refined to "gravitational aggregate" for objects with low to zero RTS, conveying the notion of gravity keeping a collection of particles together, or "coherent aggregate" for objects with moderate to high RTS, something similar to a conglomerate but with no explanation about the "glue," except that it is not gravity (see Fig. 1).

In the remainder of this chapter we will outline the evidence for why we think aggregates, and gravitational aggregates in particular, exist among the small-body population in the solar system and what the implications are for the origin and evolution of these bodies. The observational evidence is presented first, with detailed theoretical considerations and discussion of origin and evolution deferred to the later sections. We will endeavor to employ the new classifi-

cation scheme as consistently as possible throughout the chapter with the hope that use of the new terms in their proper context will help solidify the definitions.

2. EVIDENCE

Recently the possibility that a large percentage of ~0.1–100-km-sized bodies in the solar system, including asteroids, are fragile gravitational aggregates has gained greater acceptance. The reason for this is the mounting evidence from observations, experiments, and simulations that such configurations are (or should be) common. In what follows we provide an overview of this evidence.

2.1. Observations

Observational evidence for gravitational aggregates comes primarily from direct optical imaging or radar. Targets for optical imaging include both the bodies themselves and the geologic record of their past existence. Some of the earliest evidence actually comes from meteorites, mesosiderites in particular, which are mixtures of mantle basalt and core iron. The presence of both mantle and core material in a single meteorite suggests gravitational reaccumulation of the parent body following catastrophic disruption (*Scott et al.,* 2001). We must turn to other evidence, however, to determine whether such bodies still exist today.

2.1.1. Comet breakup. Comet breakups, such as that of Comet D/Shoemaker-Levy 9 (SL9) at Jupiter, may offer some insight into present-day asteroid aggregates. In July 1992, SL9 passed very close to Jupiter (*Chodas and Yeomans,* 1996), well inside the tidal breakup (Roche) limit for unconsolidated water ice (*Asphaug and Benz,* 1996). *Scotti and Melosh* (1993) estimated the tidal stress on the inferred parent body and found it to be so small (~10^{-4} bar) that the comet was likely an incoherent aggregate of fragments before breakup. *Asphaug and Benz* (1994) used an N-body code to model the gravitational forces between the constituent fragments and found that the tidal encounter elongated the rubble pile until it suffered "clump instabilities" that formed a fragment train reminiscent of SL9. Tidal breakup simulations of rubble pile asteroids show similar behavior (section 3.2).

Other comet breakups have been observed, the bulk of which were apparently caused by spontaneous nucleus splitting (*Weissman,* 1982). The most recent example is the breakup of Comet C/1999 S4 (LINEAR) (*Weaver et al.,* 2001). Some other tidal disruptions are known, however: P/Brooks 2 broke into at least eight fragments when it approached within 2 jovian radii of Jupiter in 1886 (*Sekanina and Yeomans,* 1985); various Sun grazers may also have been broken up by tides (*Weissman,* 1980; *Sekanina,* 2000).

2.1.2. Crater chains. Crater chains, or catenae, are linear configurations of up to several dozen equally spaced, similarly sized impact craters spread out over tens of kilometers. They are distinguished from endogenic features by the well-defined rims on the regular and circular craters, and the presence of chains in nonvolcanic regions (*Wichman and Wood,* 1995; *McKinnon and Schenk,* 1995). Some crater chains are known to have formed from the ejecta of a single impact event owing to their radial alignment with respect to a nearby large crater. But there are about a dozen crater chains on Ganymede and Callisto (*Schenk et al.,* 1996), and even one or two on our own Moon (*Melosh and Whitaker,* 1994; *Wichman and Wood,* 1995), that have no obvious source crater. [*Schenk et al.* (1996) found several potential crater chains on the saturnian satellites Dione, Rhea, Enceladus, and Triton, but they are all either severely degraded or in historically active regions. *Asphaug and Benz* (1996) do not think SL9-type disruption can occur near Saturn because of the planet's low density.]

Melosh and Schenk (1993) and *Bottke et al.* (1997) have suggested that these catenae are impact signatures of SL9-like fragment trains. In this scenario, a tidally disrupted body strikes one of the planet's moons on the outbound orbit, several hours to a few days after disruption. This is long enough for distinct clumps to form through instability and yet short enough for the fragment train to form a recognizable crater chain. The spacing of the craters is a function of the somewhat random orientation of the train with respect to the impact surface. The absence of any correlation between the inferred parent body mass and the number of craters in the catena supports the idea that the fragments reaccumulated via gravitational instability just prior to impact (*Asphaug and Benz,* 1996; *Schenk et al.,* 1996). *Bottke et al.* (1997) find that Earth-crossing asteroids could be pulled apart by tides if the bodies are sufficiently weak, and therefore may account for the presence of one or two crater chains on the Moon since the late heavy bombardment. Suggestions of crater chains formed on Earth by tidal disruption of an asteroid by the Moon (e.g., *Rampino and Volk,* 1996; *Ocampo and Pope,* 1996; *Spray et al.,* 1998) are discounted by *Bottke et al.* (1997) because in their model they find that, owing to the Moon's smaller size and density, for every crater chain on Earth there should be dozens of fresh crater chains on the Moon.

2.1.3. Doublet craters. Roughly 10% of the largest (mean diameter $D \geq 20$ km) impact structures on the Earth and Venus, and 2% on Mars, are doublet craters, i.e., well-separated pairs of similarly sized craters that formed simultaneously (*Bottke and Melosh,* 1996a,b). The craters are too separated (for their size) to have been formed by tidal disruption or aerodynamic breakup of an asteroid just prior to impact since these forces do not give the components sufficient tangential separation during the short interval before collision (*Melosh and Stansberry,* 1991). Also, shallow impact angles can be ruled out by the lack of crater elongation. *Bottke and Melosh* (1996a,b) argue that the impactor must be a binary with well-separated components before the final impact encounter. They showed that tidal disruption of a gravitational aggregate (modeled as a simple two-component contact binary) by a terrestrial planet could

result in detached components that evolve to larger separation via repeated distant encounters with terrestrial planets, or through mutual tidal interactions. Combining their code with a Monte Carlo code based on the work of *Chauvineau et al.* (1995), they found that ~15% of kilometer-sized Earth- and Venus-crossing asteroids and ~5% of solely Mars-crossing asteroids evolve into well-separated binaries (the Mars fraction is smaller due to the relative inefficiency of its cross section at causing tidal disruption). They further showed that a steady-state population of binaries from tidal fission and disruption events could account for the present fraction of doublets on Venus, Earth, and Mars, and could imply a sizable percentage of doublets on the Moon (~10%) and Mercury (~5%) as well (the actual number has not been determined due to the difficulty in distinguishing doublets from the saturated small-crater population on these bodies).

2.1.4. Spins. Recent measurements of asteroid spin periods from lightcurve analysis have placed interesting constraints on asteroid properties. *Pravec and Harris* (2000) analyzed data for 750 main-belt, near-Earth, and Mars-crossing asteroids. They found that the smallest asteroids (mean diameter D between 0.2 and 10 km, inferred from the mean visual magnitude assuming an average albedo consistent with the asteroid classes studied) have a nearly bimodal distribution of fast and slow rotators, unlike larger asteroids, which have a more Maxwellian distribution of spins. The small, fast rotators typically have small lightcurve amplitudes, indicating a tendency toward spherical shapes. Most importantly, there is a sharp cutoff at 2.2 h: No asteroid larger than 200 m has been observed spinning faster than this limit, which corresponds roughly to the critical breakup period for a strengthless body of bulk density ~3 g cm^{-3} (e.g., *Weidenschilling,* 1981). Since *a priori* there is no reason why a strong body would be precluded from spinning faster than this limit, the authors conclude that few (if any) asteroids larger than 200 m have tensile strength. There are, however, some very small asteroids (D < 200 m) with spin periods as fast as 2.5 min (*Pravec et al.,* 2002); these objects must have some tensile strength, though they need not be monoliths. Interestingly, sizes of a few hundred meters are thought to lie at the transition between the strength and gravity regimes of crater formation (see section 2.3).

2.1.5. Underdense asteroids. Another surprising recent observation is the apparent underdensity of some C-class asteroids. Such asteroids, found primarily in the inner part of the main belt (*Britt and Consolmagno,* 2000), are thought by virtue of their similar spectral and albedo characteristics to be the sources of carbonaceous chondrites (mean density ~2.6 g cm^{-3}; *Flynn et al.,* 1999; *Burbine et al.,* 2002). However, the *NEAR Shoemaker* spacecraft, on its way to 433 Eros, passed close enough to C-class asteroid 253 Mathilde (dimensions 66 × 48 × 44 km) to obtain a detailed shape model of the visible portion along with a mass estimate of the body, which together imply a bulk density of 1.3 ± 0.2 g cm^{-3} (*Yeomans et al.,* 1997; *Veverka et al.,* 1997, 1999; *Thomas et al.,* 1999; *Cheng et al.,* 2002). If Mathilde consists mostly of chondritic material, then the effective porosity is ~40%. As discussed in section 2.3, porosities of 20–40% can result if a body is completely shattered and reassembled, creating a gravitational aggregate. The underdensity is not believed to be due to embedded water ice because no hydrated materials were detected during the flyby (*Veverka et al.,* 1999).

There have been several other recent asteroid density measurements, some owing to advances in groundbased observation (cf. *Merline et al.,* 2002). *Merline et al.* (1999) reported on the discovery of a 13-km satellite (dubbed "Petit Prince") orbiting main-belt asteroid 45 Eugenia, a C- or F-class asteroid with an estimated mean diameter of ~215 km. The 4.7-d orbit of the satellite implies a bulk density for Eugenia between 1.2 and 1.8 g cm^{-3}, depending on the shape of the asteroid. In subsequent observations *Merline et al.* (2000) found a companion to 762 Pulcova, implying a bulk density of 1.8 g cm^{-3}. Lightcurve measurements have also revealed binaries with sufficient precision to estimate bulk densities: *Pravec et al.* (1998) find a bulk density of 1.7 g cm^{-3} for the primary of the Apollo asteroid system 1991 VH by inferring a companion from mutual eclipse events; *Pravec and Hahn* (1997) also estimate a bulk density of 1.7 g cm^{-3} for 1994 AW1, although this value is less certain; and *Mottola and Lahulla* (2000) find a bulk density of 1.4 g cm^{-3} for C-class asteroid 1996 FG3. Again, such low densities imply high porosities for these asteroids.

It is also worth noting that the bulk densities of the martian satellites Phobos and Deimos, thought to be captured C/P/D-class asteroids, are below 2 g cm^{-3} (*Hartmann,* 1990; *Kieffer et al.,* 1992; *Smith et al.,* 1995; *Murchie and Erard,* 1996). Some S-class asteroid densities have been measured by spacecraft: 2.6 ± 0.5 g cm^{-3} for 243 Ida (*Belton et al.,* 1995), thanks to the discovery of its satellite Dactyl by the *Galileo* spacecraft, and ~2.7 g cm^{-3} for 433 Eros (*Yeomans et al.,* 2000), by virtue of the *NEAR Shoemaker* orbiter (*Cheng et al.,* 2002). The higher densities imply lower porosities for these asteroids (although some of their components do contain Fe), but the values are not inconsistent with fractured or shattered configurations of low strength.

2.1.6. Giant craters. About 50% of small objects imaged to date have "giant" craters with diameters on the order of the radius of the object (*Thomas,* 1999). The most intriguing example is 253 Mathilde (section 2.1.5), which has at least four craters in this category (*Veverka et al.,* 1999; *Chapman et al.,* 1999). Mathilde also apparently lacks ejecta blankets and other global signatures of the large impacts such as fracturing and erasure of older craters. These findings support both the compaction and excavation models for crater formation on Mathilde (sections 2.2 and 2.3). Note that Mathilde is unusual in at least one other respect: It is currently the third slowest rotator known, with a spin period of 17.4 d, and is also in a tumbling state (*Mottola et al.,* 1995).

Other examples of giant craters on small bodies imaged by spacecraft include one ~23-km crater and five ~10-km

craters on S-class asteroid 243 Ida (dimensions 60 × 26 × 18 km; *Belton et al.,* 1994, 1995; *Thomas et al.,* 1996); as many as eight ~4-km or larger craters on 951 Gaspra (dimensions 18 × 11 × 9 km; *Belton,* 1994; *Greenberg et al.,* 1994); the 11-km Stickney Crater on the martian moon Phobos (dimensions 27 × 22 × 19 km; *Asphaug and Melosh,* 1993; *Murchie and Erard,* 1996); and possibly the 10-km concavity on the other martian moon, Deimos (mean radius ~6.2 km; *Thomas et al.,* 1996).

Numerical hydrocode models of asteroid collisions (section 2.3) suggest that craters this large relative to the body size could have formed only in weak or fragmented targets capable of absorbing the collision energy close to the impact site. A solid monolithic body would have been completely disrupted, erasing any sign of a crater (cf. Fig. 1). High-resolution spacecraft observations of some of these bodies support this conclusion. Crater saturation on the surface and the irregular shape of Ida suggest an internal structure that is at least megaregolith or possibly large blocks covered by rubble (*Chapman et al.,* 1996a; *Greenberg et al.,* 1996; *Sullivan et al.,* 1996). Similarly, Gaspra is probably covered with megaregolith but its lumpy structure is also consistent with a blocky interior (*Greenberg et al.,* 1994; *Chapman et al.,* 1996b).

2.1.7. Grooves. Another feature indicating that the asteroids we know best are at least partially fractured is the apparently universal occurrence of linear grooves on their surfaces. First discovered in Viking images of Mars' satellite Phobos (*Veverka and Duxbury,* 1977), grooves are mostly rimless, sometimes beaded linear depressions that have been observed on every asteroid for which we have high-resolution images: Gaspra (*Veverka et al.,* 1994), Ida (*Belton et al.,* 1994), and most recently Eros (*Veverka et al.,* 2001). These grooves are currently believed to form where loose, incohesive regolith drains into underlying gaping fissures (*Thomas et al.,* 1979). The grooves' width and the spacing of beads along them are proportional to the depth of the regolith (*Horstman and Melosh,* 1989). Their lengths indicate the lateral continuity of the fissures that underlie them. The fissures may not have been initially formed by impacts, but they probably open every time a large impact jostles the interior of the asteroid, so the grooves may postdate the fissures themselves. The internal volume created by the fissures is at least as large as the volume deficit of the grooves themselves. Physical experiments suggest that large voids may develop beneath blocks trapped in the narrow fissures, so the internal void space could be larger. The presence of grooves on an asteroid thus suggests that its interior is coherent but fractured, and so its tensile strength is reduced from that of a pristine body and that there must be voids within the asteroid, increasing its porosity.

2.1.8. Unusual shapes and binaries. Delay-Doppler radar imaging of near-Earth asteroids (*Ostro,* 1993; *Ostro et al.,* 2002) has revealed some unusual asteroid shapes: 4769 Castalia (*Ostro et al.,* 1990; *Hudson and Ostro,* 1994), 4179 Toutatis (*Ostro et al.,* 1999), 2963 Bacchus (*Benner et al.,* 1999), 12 Victoria (*Mitchell et al.,* 1995), and 216 Kleopatra (the "dogbone" asteroid; *Ostro et al.,* 2000) have distinct lobes, while 1620 Geographos (*Ostro et al.,* 1995) — the most highly elongated body known in the solar system (aspect ratio ~2.8:1) — has a shape reminiscent of a porpoise. The *NEAR Shoemaker* mission revealed 433 Eros to be somewhat kidney-bean shaped, with a large saddle depression in the middle (*Zuber et al.,* 2000). In some cases, like Geographos and Eros, the spin rate is so high the effective gravity at the extreme ends is close to zero. In contrast, Toutatis is a slow, tumbling rotator, like Mathilde. Castalia and Bacchus look very much like contact binaries. Finally, Kleopatra, an M-class asteroid, has a very high density at the surface (3.5 g cm^{-3} as inferred from the radar reflectivity), consistent with its metallic composition, but shows no slopes in excess of the angle of repose for typical grains (~34°–37°). This, together with the overall shape, led *Ostro et al.* (2000) to speculate that Kleopatra is a metallic rubble pile. [Recently *Viateau* (2000) found a bulk density of 1.8 ± 0.8 g cm^{-3} for M-class asteroid 16 Psyche from astrometric measurements. However, the moderately high radar albedo implies a surface bulk density of $2.8^{+0.5}_{-0.6}$ g cm^{-3} (C. Magri, personal communication, 2001). These values are marginally consistent, but may suggest size sorting in the surface layers (cf. *Britt and Consolmagno,* 2001)]. In much earlier work based on lightcurves, *Weidenschilling* (1980) suggested that Kleopatra is a contact or close binary and that Trojan asteroid Hektor is a close binary (*Cruikshank et al.,* 2000, suggest Hektor may be a contact binary).

Simulations of "mild" asteroid tidal disruption, for which mass loss is minimal but significant reshaping still occurs, have given rise to distinctive shapes like Geographos and Eros (section 3.3). Contact binaries and dumbbell/dogbone shapes are a natural byproduct of tidal fission (section 3.2) or damping low-speed collisions (section 3.4). These results are all facilitated by a loose aggregate structure among the progenitors.

The near-spherical shapes of many fast rotators inferred from low-amplitude lightcurves (*Pravec and Harris,* 2000) must also be considered unusual since solid bodies smaller than a few hundred kilometers cannot be rounded by gravity. A more fluid body on the other hand, i.e., a gravitational aggregate, can relax to a spherical shape during the reaccumulation process following collisional or tidal breakup. However, to maintain a spherical shape with fast spin, friction and particle size effects are needed to prevent rotational flattening.

Radar, high-resolution optical imaging, and lightcurve observations are also revealing for the first time the presence of asteroid satellites (about 10 known so far), with an extrapolated frequency of a few percent among the main-belt population and ~10–20% among near-Earth asteroids (*Pravec et al.,* 2002). Interestingly, *Pravec and Harris* (2000) find that a significant fraction of the observed (near-Earth) population of fast rotators are binaries. Binaries provide the best possible measure of the primary mass (strictly, the sum of the masses), and together with shape estimates these lead to bulk density determinations, revealing in many cases some surprisingly low values (section 2.1.5).

2.2. Experiments

Naturally the best way to understand asteroids, aggregate asteroids in particular, is to study them *in situ*. Recently researchers have carried out successful flybys of several asteroids (Ida, Gaspra, Mathilde) and even managed a landing on one (Eros). In 2005, the *Deep Impact* spacecraft will fire a 350-kg projectile into Comet P9 Temple 1. Taking this one step further, an ideal but expensive mission would include detailed seismic measurements from multiple points on the surface of an asteroid to deduce the interior structure. However, it is also possible to gain insight into asteroid properties through carefully conceived experiments in laboratories on Earth, despite practical restrictions on impactor sizes and speeds. For example, experimentalists can investigate the effect of porosity on collision outcome, or even simulate the gravity regime with a centrifuge.

Typically, experimentalists find that asteroids with low strength and/or high porosity can damp impact energy more effectively than their stronger, less porous counterparts, a conclusion shared by numerical modelers (section 2.3). For example, *Love et al.* (1993) conducted hypervelocity experiments using targets of variable porosity and found that the more porous targets had deeper craters, lower ejecta velocities, and less distal damage. They concluded that porosity is an effective damper of impact energy and could be an important factor in calculating the lifetimes of small solar system objects. *Ryan et al.* (1991) dropped objects made of shattered concrete fragments held together by glue and found these resisted impact damage a factor of 2–3× more efficiently than the original concrete. They attributed this characteristic to energy dissipation.

Two convenient measures of impact outcomes are the critical specific shattering energy, Q^*_S, and dispersing energy, Q^*_D (*Durda et al.,* 1998; also see *Davis et al.,* 1979, for an earlier convention). Q^*_S is the projectile kinetic energy per unit target mass required to shatter the target so that the largest intact fragment contains 50% of the target mass. Q^*_D is the specific energy required to shatter and permanently disperse the target against gravity so that the largest (possibly reaccumulated) fragment has 50% of the target mass. Evidently Q^*_S is all that can be measured directly in the laboratory, since strength dominates over gravity for target sizes up to a few hundred meters. Generally Q^*_S decreases with target diameter due to the increasing likelihood of finding larger flaws in bigger bodies (*Housen and Holsapple,* 1990; *Holsapple,* 1994). Note that a body with RTS = 0 (e.g., a previously shattered body, or a rubble pile) by definition also has $Q^*_S = 0$. In the gravity regime, Q^*_S is negligible and Q^*_D dominates, increasing in value with target size as the gravity well deepens. The point where Q^*_S is comparable to Q^*_D is the transition from the strength to the gravity regime.

Housen et al. (1991) used a pressure chamber to expose a target of low strength to variable amounts of overpressure in order to simulate the stresses inside a self-gravitating asteroid, in other words, to estimate Q^*_D. Due to practical constraints, they could not conduct actual impacts with this configuration; instead they used buried explosive charges to simulate projectile impacts. They found that as the overpressure increased, the amount of material retained by the target also increased. By relating the target diameter to the amount of overpressure, they derived a Q^*_D scaling law consistent with the specific energies estimated for several asteroid families. However, the use of an explosion in place of an impact, and the 1/r scaling of pressure (instead of $1/r^2$ for gravity), introduces some uncertainty in the result, but the experiment does provide an upper bound on Q^*_D (*Holsapple,* 1994).

Another way of simulating the gravity regime on large bodies is to use a centrifuge. *Housen et al.* (1999) did this in an experiment designed to study the unusual cratering on Mathilde (section 2.1.6). A gas gun mounted on the centrifuge arm was used to impact a crushable porous target at 1.9 km s^{-1}. At 500 g the small craters formed by centimeter-sized projectiles have the same gravitational effects as the giant craters on Mathilde. They found that in this regime the impacts compacted the target material and produced almost no ejecta inside or outside the crater. They concluded that if compaction is responsible for the craters on Mathilde and other similar asteroids (no ejecta blankets were detected on Mathilde, although they would have been at the limit of resolution, and neighboring impacts appear to have produced little distal damage; cf. section 2.1.6), the characteristics of the craters are governed by neither strength nor gravity but rather the crushing material property of the target itself. For significant compaction to occur in silicates, densities must be below 2 g cm^{-3}. If compaction is the relevant mechanism on Mathilde, the five impacts that created the giant craters increased its bulk density by about 20%. This suggests that over time a porous body could be processed into a denser object. This mechanism also suggests that porous, compactable bodies are not efficient producers of meteorites, since most of the material is retained. This is in contrast to numerical studies that suggest excavation is highly efficient in porous bodies (section 2.3).

2.3. Simulations

The final piece of evidence concerning the existence of aggregate asteroids comes from direct numerical simulations, which in many respects are simply theoretical experiments. The two most common approaches use hydrodynamic codes, where state variables such as pressure and temperature are followed explicitly, and particle codes, where only gravity and collisions are considered. The former are better suited for modeling short-term stresses such as hypervelocity impacts (where fracturing, crushing, and melting are important) while the latter are optimal for studying long-term stresses such as tidal disruption or very low speed collisions (where the evolution takes place over many dynamical times). In this section only those experiments designed to compare the reaction of solid and aggregate bodies to short-term stresses will be discussed. Simulations that start solely from the premise of aggregate bodies are discussed in section 3.

Since laboratory experiments are limited to very small impactor sizes and only moderate velocities, numerical

simulations are used to extrapolate over the many orders of magnitude in energy represented by typical collisions between small bodies in the solar system. Prior to the availability of simulations, analytic scaling laws relating Q_S^* or Q_D^* were used (cf. section 2.2). In the strength regime, the function $Q_S^*(D)$ (D is the mean target diameter) depends on the adopted strength model (i.e., equation of state, distribution of flaws, etc.). In the gravity regime, $Q_D^*(D)$ in principle has a fixed power-law slope, since the fragmentation is dominated by gravity and not the strength of the constituent pieces. However, analytic scaling laws often disagree with numerical simulations on the details of these functions, largely because the former rely on simplifications needed for practical considerations (*Benz and Asphaug,* 1994; see Fig. 5 of *Holsapple et al.,* 2002, for a graphical comparison of analytical, experimental, and simulation results — estimates of the transition from the strength regime to the gravity regime vary from D ~100 m to ~10 km). Numerical simulations differ among each other as well due to simplifying assumptions of the geometry, the range of parameters tested, differences in the numerical resolution, or, in the strength regime, the adopted strength model. As computing power improves the severity of these issues will be reduced.

Perhaps the most detailed numerical model to date, spanning both the strength and gravity regimes, is the three-dimensional smoothed particle hydrodynamics (SPH) model of *Benz and Asphaug* (1999). Because their code incorporates a brittle fragmentation model, it has been calibrated with laboratory experiments, adding an element of robustness not found in previous models, although it still requires extrapolation along a power law for the size dependence (*Asphaug et al.,* 2002). They find the transition from the strength to the gravity regime occurs around D ~ 300 m, making these the weakest bodies in the solar system. *Love and Ahrens* (1996) found a similar value using a simpler SPH code for the gravity regime and extrapolating to the *Holsapple* (1994) scaling curve for the strength regime. *Melosh and Ryan* (1997) found a somewhat larger (but still small) value of D = 800 m using a Lagrangian hydrocode with a material strength model included. These results imply that most asteroids of a few hundred meters in size or larger (up to a few hundred kilometers in size, where gravity can begin to crush the interiors) may be gravitational aggregates, since the probability of a dispersing impact is far less than the probability of a shattering impact for these bodies. This provides a natural explanation for the sharp cutoff seen in asteroid spin rates at about this size (section 2.1.4). Objects below this size are presumably young intact fragments of recent collisions that have so far escaped destruction.

Benz and Asphaug (1999) show that the inefficiency of momentum transfer in collisions contributes to the steep Q_D^* power-law slope in their simulations, a finding shared by *Ryan and Melosh* (1998). Both groups also find that, for fixed collisional energy, larger projectiles are more efficient at transferring momentum, i.e., they give rise to higher fragment speeds. This has important implications for planetesimal growth (section 3.4). *Benz and Asphaug* (1999) also note that Q_D^* can be a factor of 10 larger for a head-on collision compared to a glancing collision.

In related work, *Asphaug et al.* (1998) compared the hypervelocity-impact response of a coherent body with that of a moderately fragmented (but not strengthless) porous aggregate. For realism, both bodies were shaped like 4769 Castalia (cf. section 2.1.8). They found that fractures and voids in the porous body damp the propagation of the impact shock wave, confining the deposition of energy (kinetic or thermal) to a small volume near the impact site. This can result in excavation of a large crater and ejection of material at the impact site, perhaps beyond the surface escape speed, so there is no ejecta blanket and little evidence of the impact elsewhere on the body. Such a scenario may explain the giant craters on Mathilde (section 2.1.6; *Asphaug et al.,* 2002). In a solid body, the shock wave propagates freely so there is less energy deposition at the impact site and the collision may lead to extensive fracturing and distal damage. The authors conclude that the first impact to significantly fragment an asteroid will determine much of its subsequent collisional evolution. For compound bodies, such as a contact binary or a solid body with a deep regolith mantle, impact energy may be confined to one component, i.e., one lobe in the case of a contact binary, assuming there is an impedance barrier of rubble between the two lobes, or to the regolith in the second example. Evidently a detailed knowledge of the internal properties of an asteroid is required to fully predict, for instance, its response to nuclear explosions for the purpose of hazard mitigation, or even for understanding small-body evolution.

Finally, numerical simulations of hypervelocity impacts have revealed that reaccumulation of gravitationally bound material following a catastrophic collision can create objects with moderate porosities, between 20% and 40% (*Wilson et al.,* 1999; cf. "shattered with rotated components," Fig. 1). Since this high porosity impedes energy transmission through the body, subsequent impacts may not greatly alter the porosity. Moreover, although small-scale collisions may generate new regolith on the surface, it may be that friction prevents the small particles from filtering into the void spaces (*Britt and Consolmagno,* 2001; *Britt et al.,* 2002). Perhaps moderate-scale collisions provide the only mechanism for lowering the porosity, by gradually collapsing void spaces without ejecting much material.

3. EVOLUTION

Having established various lines of evidence that asteroids with low tensile strength and a range of porosity may exist in the solar system, we now consider the origin and evolution of these bodies.

3.1. Origin

Numerical simulations have shown that solid bodies can be completely shattered by hypervelocity ($\geq$1 km s^{-1}) impacts without being dispersed (section 2.3). Moreover, the larger a body is, beyond ~100 m or so, the more likely it is

to be shattered before ever being dispersed. This is because the critical dispersal energy is a steep function of the target diameter and the size distribution of impactors is a power law with large negative exponent (*Davis et al.,* 1989). In addition, the first shattering, nondispersive impact creates a body with even greater resistance to disruption. This then is a natural explanation for the origin of gravitational aggregates in the solar system, at least among the asteroid population: The long collisional history of such bodies suggests they suffered a shattering impact in their past. This does not preclude the possibility that asteroids (and comets; cf. *Weidenschilling,* 1994, 1997) were actually born with a very loosely consolidated structure. For example, planetesimal growth via gravitational instabilities could lead naturally to aggregate structure (*Ward,* 2000). But many asteroids, particularly those ~100 km or smaller, most likely have suffered at least one shattering impact during their lifetime (*Davis et al.,* 1989; *Bottke et al.,* 1994).

Of related interest is the origin of binary asteroids (section 2.1.8). Although such systems may be long lived, it is unlikely they have survived for the age of the solar system. [*Chapman et al.* (1996a) suggest Ida/Dactyl may be a few billion years old, but *Davis et al.* (1996) note that Dactyl, due to its small size, may have suffered several completely disruptive impacts while orbiting Ida.] Instead binaries probably formed more recently. Gravitational capture of a satellite can be ruled out since it requires a special mechanism such as an improbable interaction with a third body to extract energy from the otherwise hyperbolic encounter orbit. Collisions would occur more frequently than such chance encounters. Tidal disruption could work for bodies that approach terrestrial planets (cf. section 2.1.3), but cannot explain the main-belt binaries [even if there were terrestrial planets in the main-belt region in the past (cf. *Chambers and Wetherill,* 2001), they were ejected long ago]. Retention of ejecta in orbit following a moderately dispersive collision is a possible way to create tiny satellites (e.g., Ida/Dactyl, Eugenia/Petit Prince; cf. section 3.4) since this involves a many-body ($N > 3$) interaction in which escaping ejecta carries away energy, leaving some material in orbit. This mechanism cannot produce orbiting components of near-equal size, however; these must always fall back to produce at best a contact binary since there is insufficient escaping mass to alter the essentially two-body interaction of the components. The most promising explanation for binaries of any mass ratio is that they were mutually captured following a highly dispersive impact into a much larger body (*Durda,* 1996; *Greenberg et al.,* 1996; *Michel et al.,* 2001). This suggests that binary asteroids may be reaccumulated gravitational aggregates as a result of the catastrophic impacts that formed them. So far the low bulk densities measured for binary asteroids supports this conclusion (section 2.1.5).

3.2. Tidal Breakup

The observed breakup of comets (section 2.1.1) has led to speculation about whether dense terrestrial planets could play a significant role in the evolution of asteroids via tidal encounters. The familiar Roche criterion for tidal breakup (cf. *Chandrasekhar,* 1969) implies, for example, that a body with a bulk density of 2 g cm^{-3} and no tensile strength can be disrupted if it passes within 3.4 $R_\oplus$ of Earth's center, where $R_\oplus$ is Earth's radius. The Roche limit in general applies only to synchronous rotating liquid satellites in circular orbit. *Sridhar and Tremaine* (1992) extended Roche's treatment to nonrotating viscous bodies undergoing parabolic encounters and found the disruption limit to be about two-thirds smaller than the Roche limit. *Asphaug and Benz* (1994) confirmed this value in their simulations of the SL9 breakup. Later, *Asphaug and Benz* (1996) generalized their results to obtain a scale-invariant description of tidal encounters, finding that the same tidal outcome will result for the same ratio of periapse distance to Roche limit (for parabolic encounters with nonrotating spherical bodies). In earlier work on the tidal disruption of planetesimals by terrestrial planets, *Boss et al.* (1991) used an SPH model to show that Earth's tidal forces can cause planetesimal mass shedding, sometimes even resulting in SL9-like outcomes. More recently, *Bottke and Melosh* (1996a,b) invoked tidal fission of rotating contact binaries by terrestrial planets to explain the doublet crater population (section 2.1.3).

In an attempt to explore the possible outcomes of tidal encounters between strengthless asteroids and the Earth more fully, *Richardson et al.* (1998) performed hundreds of simulations using a particle-based N-body code. Starting with kilometer-sized spheroidal and ellipsoidal progenitors of 2 g cm^{-3} bulk density each made up of 247 identical 3.6 g cm^{-3} self-gravitating spheres, they investigated the encounter outcome as a function of periapse, speed at infinity, spin period, spin axis orientation, and phase angle at periapse. All encounters were hyperbolic and covered a range of speeds representative of the near-Earth asteroid population. A hard-sphere model with dissipation was used for treating particle collisions. Generally the outcome was found to be only weakly sensitive to the amount of dissipation, so long as there was at least some dissipation (otherwise reaccumulation resulted in particle swarms rather than aggregates). Encounter outcomes were parameterized chiefly by the mass retained, orbiting, or escaping the largest remnant. Figure 2 shows some examples of post-tidal-encounter configurations (not previously published).

Richardson et al. (1998) found that the closer and slower the encounter, i.e., the more time spent within the tidal limit, the more violent the outcome, ranging from SL9-type disruptions (with reaccumulation into fragment trains) at one extreme to mild distortion and/or spinup at the other. The spin period and orientation also strongly affected the outcome, with fast prograde rotation assisting breakup and fast retrograde rotation resisting it. An elongated asteroid was found to be much easier to disrupt than a spherical one if the orientation (phase) of the ellipsoid was favorable at periapse (long axis rotating toward the Earth). *Richardson et al.* (1998) showed that their results can account for the presence of one or two crater chains on the Moon and none on the Earth (section 2.1.2; also see *Bottke et al.,* 1997).

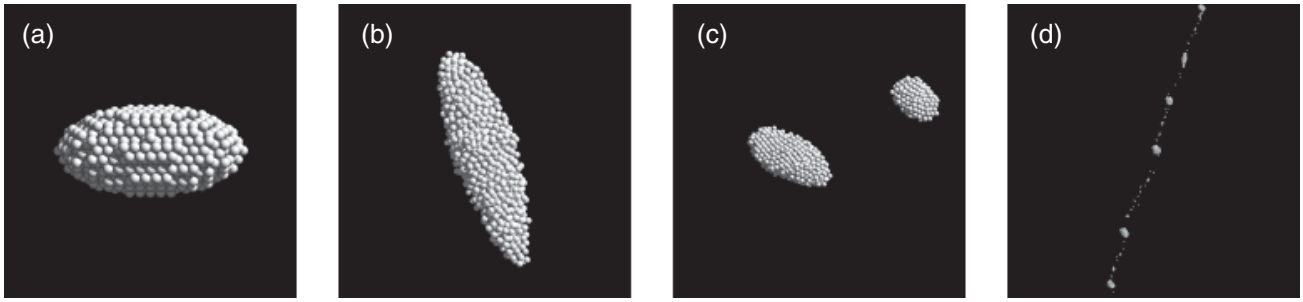

Fig. 2. Snapshots of simulated gravitational aggregate tidal encounters with Earth at different encounter speeds (close approach distance $q = 1.4\ R_\oplus$): **(a)** 4 × 2 km, 2 g cm^{-1} ellipsoidal progenitor with 993 identical spheres prior to encounter; **(b)** mild disruption at encounter speed $v_\infty = 15$ km s^{-1}, stretching the progenitor to 6 km length and stripping away a few particles (not shown); **(c)** moderate disruption at $v_\infty = 12$ km s^{-1} resulting in a stable binary of mass ratio 0.36 and eccentricity 0.16; **(d)** SL9-like disruption at $v_\infty = 6$ km s^{-1} yielding 21 large fragments (not all shown).

They found that ~10% of the ejecta ends up in orbit around the largest remnant, suggesting binaries could be created by tidal disruptions. They also found that the irregular shapes of some near-Earth asteroids could be explained by tidal encounters (section 3.3). This includes double-lobed bodies such as Castalia, Bacchus, Toutatis, and Kleopatra, which may be formed by the gentle mutual reaccretion of similar-sized bodies with moderate angular momentum following a tidal breakup or a low-speed collision. Tidal disruption could also explain the enhancement of the local population of small (≤50 m) bodies (*Bottke et al.,* 1998).

3.3. Spinup and Reshaping

Even though a tidal encounter may be too weak for significant mass loss to occur, the progenitor can still suffer substantial changes to its spin or, for bodies with low tensile strength, its shape. *Solem and Hills* (1996) used a strengthless aggregate model consisting of spherical frictionless boulders to demonstrate that shapes even more elongated than Geographos (section 2.1.8) could be achieved through tidal stretching. *Bottke et al.* (1999) were able to match details of the unusual porpoise-like shape of Geographos using their model with a mild low-mass-loss tidal encounter, arguing that the orbital parameters of the Earth-crossing asteroid are favorable for past tidal encounters with the Earth or Venus. They also suggested that Eros could be shaped by planetary tides. More generally, for mild interactions, *Richardson et al.* (1998) showed that the post-encounter spin and ellipticity of the progenitor are correlated with the preencounter values: A prograde progenitor spins up a bit and becomes more elongated, a retrograde progenitor spins down and becomes more spherical. *Scheeres et al.* (2000) used a combination of analytical theory and numerical simulations to show that spin changes (including tumbling for an asteroid like Toutatis) can occur even for relatively large encounter distances, although this work does not require a low-strength progenitor. They also showed that spin states of comparable-sized bodies can be dramatically altered during the brief interval of their evolution following fragmentation from a larger body. This kind of interaction may explain the origin of the slow-rotator population among small asteroids: An escaping fragment could rob its partner of rotational energy in order to escape the system (*Harris,* 2001). Finally, nongravitational thermal forces may also play a role in changing an asteroid's spin (*Bottke et al.,* 2002).

It should be noted that comprehensive numerical studies of allowed shapes and spin states of gravitational aggregates, including a determination of the damping time to principal axis rotation, have not yet been performed. Analytical models that approximate asteroids as fluid Maclaurin spheroids or Jacobi ellipsoids (cf. *Binney and Tremaine,* 1987) have been available for some time (*Weidenschilling,* 1981; *Farinella et al.,* 1981; both studies demonstrated that asteroid spin and shape are diagnostic of strength and porosity), but it remains to compare these in detail with numerical models, even those restricted to simple spheres with dissipation and surface friction without normal resting forces. More sophisticated models with irregular particle shapes and rolling and sliding modes are still a long way off.

3.4. Impacts

Hydrocode models of hypervelocity impacts into aggregate asteroids were discussed in section 2.3. It was shown that porous or damaged structure damps impact energy very efficiently, shielding the rest of the asteroid from damage. A solid body, on the other hand, may be completely shattered by a high-speed impact and yet retain most of its material if it has enough mass. At even higher impact energies, dispersal will occur, but the ejecta can reaccumulate into smaller aggregate bodies. *Durda* (1996) proposed this mechanism to explain the origin of the Ida/Dactyl system (cf. section 3.1), which is a member of the Koronis family. (Asteroid families share similar physical and dynamical characteristics and are thought to have originated from catastrophic disruptions of a single larger body; see the chapters on asteroid families in this volume for a com-

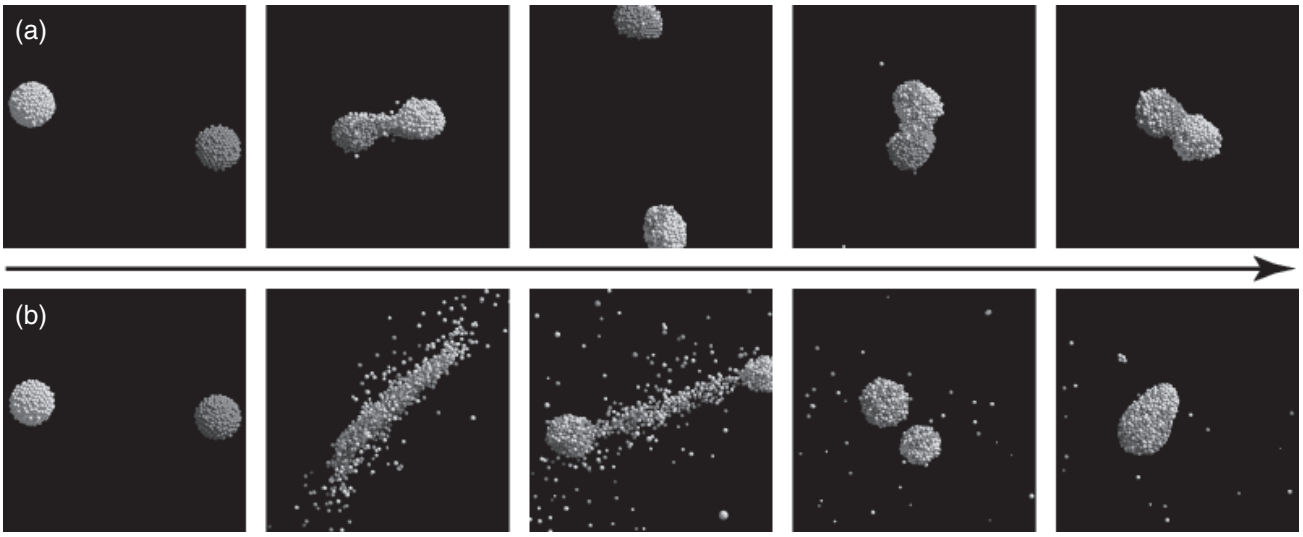

Fig. 3. Simulations of collisions between kilometer-sized gravitational aggregates: **(a)** impact angle $\phi \sim 60°$, impact speed $v_c \sim v_e$ (v_e is the escape speed from one body, ~1 m s^{-1} in this case), resulting in a contact binary; **(b)** $\phi \sim 17°$, $v_c \sim 2.5\ v_e$, opposite 6-h spins, giving rise to a teardrop-shaped aggregate with a tiny reaccumulated satellite (upper left). See *Leinhardt et al.* (2000) for more details.

prehensive review.) *Campo Bagatin and Petit* (2001) used a semianalytical approach to argue that gravitational aggregates in the size range of 10–100 km should be common in the asteroid belt. Recently *Michel et al.* (2001) combined an SPH fragmentation code with an N-body gravity code to show that hypervelocity impacts can form systems that resemble asteroid families and that during this process many binaries can form. In their simulations they found that family-forming impacts always completely shattered the target, yet postimpact reaccumulation gave rise to a mass spectrum and velocity distribution that were a good match for present-day families (allowing for erosional and dynamical evolution). They concluded that large family members must be gravitational aggregates consisting of reaccumulated fragments. This result resolves the long-standing dilemma that family members, previously believed to be solid fragments, have ejection speeds too high for the fragments to have survived the family-forming impact intact.

It is also of interest to consider the response of gravitational aggregates to low-speed collisions (≲100 m s^{-1}). Low encounter speeds are appropriate during the planetesimal growth phase, when relative speeds are on the order of the surface escape speed for the most gravitationally dominant body, e.g., ~1 m s^{-1} for a body of 1 km radius and 2 g cm^{-3} bulk density. Low collision speeds may also be relevant during the reaccumulation phase following a catastrophic impact. Using an SPH code that incorporates material strength and brittle fracture, *Benz* (2000) found that low-speed collisions between equal-sized bodies (both weak and strong) are surprisingly more efficient at fragmentation and dispersal than high-speed collisions for equal projectile kinetic energy per unit target mass. The reason is that momentum transfer is more efficient in collisions involving bodies of comparable size. *Benz* (2000) suggests that this relative fragility may hamper planetesimal growth in the 1-m to 1-km size range.

Leinhardt et al. (2000) found similar results using an N-body particle code (see *Richardson et al.,* 2000, for code details). In this study, kilometer-sized strengthless gravitational aggregates comprised of 955 identical spherical particles were collided at speeds less than 10 m s^{-1} (see Fig. 3 for some snapshots). Various spin configurations were sampled, with a range of impact angles and impact speeds for each. The impactors were of equal size except in one model where a mass ratio of 10:1 was used. They found that higher impact speeds (kinetic energy) yielded smaller remnant sizes and greater mixing, while larger impact angles (angular momentum) generated fast-spinning elongated or double-lobed remnants. Critical disruption was found to occur at roughly 4× the gravitational binding energy for these bodies. When initial spins were oppositely oriented, triaxial remnant shapes sometimes formed. The results were sensitive to the value of the dissipation parameter, with greater dissipation yielding larger remnant masses and more efficient clumping overall. The results were not sensitive to the numerical resolution: Simulations with 5× as many particles gave results similar to the low-resolution cases for the same impact parameters. The largest mass accumulation found orbiting the remnant in these simulations was ~2% of the total mass (fragments orbiting bodies smaller than the largest remnant were not searched for). Collisions between objects of equal size were found to result in net accretion 35% of the time (for a nominal value of the dissipation parameter), indicating that these bodies are relatively fragile. Again this may imply there is a bottleneck for planetesimal growth at small sizes, unless the growth mode is predominantly through collisions between bodies of large mass ratio. Although planetesimals of different

mass typically have higher collision speeds owing to size-dependent gas drag effects (*Weidenschilling and Cuzzi,* 1993), the critical disruption energy is also higher for these cases, so accretion may still be favored (*Leinhardt and Richardson,* 2002).

4. CONCLUSIONS

Many, if not most, kilometer-sized asteroids (and comets) in the solar system may be gravitational aggregates of low tensile strength. Growth of planetesimals via collective instabilities may have led to aggregate structure, but even if asteroids were solid at one time in the past, repeated impacts over their lifetimes have likely shattered them by now. Once broken up, an asteroid can absorb impacts more efficiently, improving its survival chances. Apart from these theoretical and experimental considerations, the existence of gravitational aggregates is supported by observations: The cometary breakups that have been directly witnessed indicate very weak structures for these primordial bodies; crater chains on the Moon are consistent with tidal breakup of weak asteroids by the Earth; the doublet crater population on Earth, Venus, and Mars can be understood in terms of asteroid binary formation via tidal fission; the sharp asteroid spin-rate cutoff suggests asteroids larger than a few hundred meters cannot support tension; low bulk densities measured for several asteroids imply high porosities that can be explained by the reassembly of fragments; the presence of giant craters on several asteroids indicates efficient damping or compaction at the surface, consistent with damaged, rubblized, or highly porous and compactable structures; grooves imaged on asteroids suggest regolith drainage between fractured blocks; the unusual shapes of some asteroids can be explained by tidal stripping or shaping; and recent observations of binary asteroids suggest they may have formed from reaccumulated fragments following catastrophic disruptions of larger bodies.

Until direct seismic measurements of asteroids are made, or an extremely fortuitous observable collision or tidal breakup occurs, evidence for gravitational aggregates will remain largely circumstantial. This means the onus is on experimentalists and theorists to improve their models of the mechanical and dynamical properties of aggregate configurations. As the weight of evidence increases, even the most stubborn of skeptics will be convinced that gravitational aggregates play a crucial role in our understanding of the solar system.

Acknowledgments. The authors thank A. Campo Bagatin and D. Davis for their critical reviews of the manuscript. We also wish to thank the many contributors to section 1 in the wake of the Asteroids 2001 meeting. We hope we got it right!

REFERENCES

Asphaug E. and Benz W. (1994) Density of Comet Shoemaker-Levy 9 deduced by modelling breakup of the parent "rubble pile." *Nature, 370,* 120–124.

Asphaug E. and Benz W. (1996) Size, density, and structure of Comet Shoemaker-Levy 9 inferred from the physics of tidal breakup. *Icarus, 121,* 225–248.

Asphaug E. and Melosh H. J. (1993) The Stickney impact of Phobos: A dynamical model. *Icarus, 101,* 144–164.

Asphaug E., Ostro S. J., Hudson R. S., Scheeres D. J., and Benz W. (1998) Disruption of kilometre-sized asteroids by energetic collisions. *Nature, 393,* 437–440.

Asphaug E., Ryan E., and Zuber M. (2002) Asteroid interiors. In *Asteroids III* (W. F. Bottke Jr. et al., eds.), this volume. Univ. of Arizona, Tucson.

Belton M. J. S. (1994) Galileo encounter with 951 Gaspra: First pictures of an asteroid. *Science, 257,* 1647–1652.

Belton M. J. S. and 19 colleagues (1994) First images of asteroid 243 Ida. *Science, 265,* 1543–1547.

Belton M. J. S. and 12 colleagues (1995) Bulk density of asteroid 243 Ida from the orbit of its satellite Dactyl. *Nature, 374,* 785–788.

Benner L. A. M. and 12 colleagues (1999) Radar observations of asteroid 2063 Bacchus. *Icarus, 139,* 309–327.

Benz W. (2000) Low velocity collisions and the growth of planetesimals. *Space Sci. Rev., 92,* 279–294.

Benz W. and Asphaug E. (1994) Impact simulations with fracture. I. Method and tests. *Icarus, 107,* 98–117.

Benz W. and Asphaug E. (1999) Catastrophic disruptions revisited. *Icarus, 142,* 5–20.

Binney J. and Tremaine S. (1987) *Galactic Dynamics.* Princeton Univ., Princeton, New Jersey. 733 pp.

Bockelée-Morvan D. and 11 colleagues (2001) Outgassing behavior and composition of Comet C/1999 S4 (LINEAR) during its disruption. *Science, 292,* 1339–1343.

Boss A. P., Cameron A. G. W., and Benz W. (1991) Tidal disruption of inviscid planetesimals. *Icarus, 92,* 165–178.

Bottke W. F. Jr. and Melosh H. J. (1996a) Formation of asteroid satellites and doublet craters by planetary tidal forces. *Nature, 381,* 51–53.

Bottke W. F. Jr. and Melosh H. J. (1996b) Binary asteroids and the formation of doublet craters. *Icarus, 124,* 372–391.

Bottke W. F. Jr., Richardson D. C., and Love S. G. (1997) Can tidal disruption of asteroids make crater chains on the Earth and Moon? *Icarus, 126,* 470–474.

Bottke W. F. Jr., Richardson D. C., and Love S. G. (1998) Production of Tunguska-sized bodies by Earth's tidal forces. *Planet. Space Sci., 46,* 311–322.

Bottke W. F. Jr., Nolan M. C., Greenberg R., and Kolvoord R. A. (1994) Velocity distributions among colliding asteroids. *Icarus, 107,* 255–268.

Bottke W. F. Jr., Richardson D. C., Michel P., and Love S. G. (1999) 1620 Geographos and 433 Eros: Shaped by planetary tides? *Astron. J., 117,* 1921–1928.

Bottke W. F. Jr., Vokrouhlický D., Rubincam D. P., and Brož M. (2002) The effect of Yarkovsky thermal forces on the dynamical evolution of asteroids and meteoroids. In *Asteroids III* (W. F. Bottke Jr. et al., eds.), this volume. Univ. of Arizona, Tucson.

Britt D. T. and Consolmagno G. J. (2000) The porosity of dark meteorites and the structure of low-albedo asteroids. *Icarus, 146,* 213–219.

Britt D. T. and Consolmagno G. J. (2001) Modeling the structure of high porosity asteroids. *Icarus, 152,* 134–139.

Britt D. T., Yeomans D. K., Housen K. R., and Consolmagno G. J. (2002) Asteroid densities, porosities, and structures. In *Aster-*

oids III (W. F. Bottke Jr. et al., eds.), this volume. Univ. of Arizona, Tucson.

Burbine T. H., McCoy T. J., Meibom A., Gladman B., and Keil K. (2002) Meteoritic parent bodies: Their number and identification. In *Asteroids III* (W. F. Bottke Jr. et al., eds.), this volume. Univ. of Arizona, Tucson.

Campo Bagatin A. and Petit J.-M. (2001) How many rubble piles are in the asteroid belt? *Icarus, 149,* 198–209.

Chambers J. E. and Wetherill G. W. (2001) Planets in the asteroid belt. *Meteoritics & Planet. Sci., 36,* 381–399.

Chandrasekhar S. (1969) *Ellipsoidal Figures of Equilibrium.* Yale Univ., New Haven, Connecticut. 252 pp.

Chapman C. R. (1978) Asteroid collisions, craters, regolith, and lifetimes. In *Asteroids: An Exploration Assessment* (D. Morrison and W. C. Wells, eds.), pp. 145–160. NASA Conf. Publ. 2053.

Chapman C. R., Merline W. J., and Thomas P. (1999) Cratering on Mathilde. *Icarus, 140,* 28–32.

Chapman C. R., Ryan E. V., Merline W. J., Neukum G., Wagner R., Thomas P. C., Veverka J., and Sullivan R. J. (1996a) Cratering on Ida. *Icarus, 120,* 77–86.

Chapman C. R., Veverka J., Belton M. J. S., Neukum G., and Morrison D. (1996b) Cratering on Gaspra. *Icarus, 120,* 231–245.

Chauvineau B., Farinella P., and Harris A. W. (1995) The evolution of Earth-approaching binary asteroids: A Monte Carlo dynamical model. *Icarus, 115,* 36–46.

Cheng A. F. (2002) Near Earth Asteroid Rendezvous: Mission summary. In *Asteriods III* (W. F. Bottke Jr. et al., eds.), this volume. Univ. of Arizona, Tucson.

Chodas P. W. and Yeomans D. K. (1996) The orbital motion and impact circumstances of Comet Shoemaker-Levy 9. In *The Collision of Comet Shoemaker-Levy 9 and Jupiter* (K. S. Noll et al., eds.), pp. 1–30. Proc. IAU Colloq. 156, Cambridge Univ., Cambridge.

Cruikshank D. P., Dalle Ore C. M., Geballe T. R., Roush T. L., Owen T. C., Cash M., de Bergh C., and Hartmann W. K. (2000) Trojan asteroid 624 Hektor: Constraints on surface composition. *Bull. Am. Astron. Soc., 32,* 1027.

Davis D. R., Chapman C. R., Greenberg R., Weidenschilling S. J., and Harris A. W. (1979) Collisional evolution of asteroids: Populations, rotations, and velocities. In *Asteroids* (T. Gehrels, ed.), pp. 528–557. Univ. of Arizona, Tucson.

Davis D. R., Weidenschilling S. J., Farinella P., Paolicchi P., and Binzel R. P. (1989) Asteroid collisional history: Effects on sizes and spins. In *Asteroids II* (R. P. Binzel et al., eds.), pp. 805–826. Univ. of Arizona, Tucson.

Davis D. R., Chapman C. R., Durda D. D., Farinella P., and Marzari F. (1996) The formation and collisional/dynamical evolution of the Ida/Dactyl system as part of the Koronis family. *Icarus, 120,* 220–230.

Durda D. D. (1996) The formation of asteroidal satellites in catastrophic collisions. *Icarus, 120,* 212–219.

Durda D. D., Greenberg R., and Jedicke R. (1998) Collisional models and scaling laws: A new interpretation of the shape of the main-belt asteroid size distribution. *Icarus, 135,* 431–440.

Farinella P., Paolicchi P., Tedesco E. F., and Zappalà V. (1981) Triaxial equilibrium ellipsoids among the asteroids? *Icarus, 46,* 114–123.

Flynn G. J., Moore L. B., and Klöck W. (1999) Density and porosity of stone meteorites: Implications for the density, porosity, cratering, and collisional disruption of asteroids. *Icarus, 142,* 97–105.

Greenberg R., Nolan M. C., Bottke W. F. Jr., Kolvoord R. A., and Veverka J. (1994) Collisional history of Gaspra. *Icarus, 107,* 84–97.

Greenberg R., Bottke W. F. Jr., Nolan M., Geissler P., Petit J., Durda D., Asphaug E., and Head J. (1996) Collisional and dynamical history of Ida. *Icarus, 120,* 106–118.

Harris A. W. (2001) On the slow rotation of asteroids. *Icarus,* in press.

Hartmann W. K. (1990) Additional evidence about an early intense flux of C asteroids and the origin of Phobos. *Icarus, 87,* 236–240.

Holsapple K. A. (1994) Catastrophic disruptions and cratering of Solar System bodies: A review and new results. *Planet. Space Sci., 42,* 1067–1078.

Holsapple K., Giblin I., Housen K., Nakamura A., and Ryan E. (2002) Asteroid impacts: Laboratory experiments and scaling laws. In *Asteriods III* (W. F. Bottke Jr. et al., eds.), this volume. Univ. of Arizona, Tucson.

Horstman K. C. and Melosh H. J. (1989) Drainage pits in cohesionless materials: Implications for the surface of Phobos. *J. Geophys. Res., 94,* 12433–12441.

Housen K. R. and Holsapple K. A. (1990) On the fragmentation of asteroids and planetary satellites. *Icarus, 84,* 226–253.

Housen K. R., Holsapple K. A., and Voss M. E. (1999) Compaction as the origin of the unusual craters on the asteroid Mathilde. *Nature, 402,* 155–157.

Housen K. R., Schmidt R. M., and Holsapple K. A. (1991) Laboratory simulations of large scale fragmentation events. *Icarus, 94,* 180–190.

Hudson R. S. and Ostro S. J. (1994) Shape of asteroid 4769 Castalia (1989 PB) from inversion of radar images. *Science, 263,* 940–943.

Jackson J. A., ed. (1997) *Glossary of Geology,* 4th edition. American Geological Institute, Alexandria, Virginia. 800 pp.

Jeffreys H. (1947) The relation of cohesion to Roche's limit. *Mon. Not. R. Astron. Soc., 107,* 260–272.

Kieffer H. H., Jakosky B. M., and Snyder C. W. (1992) The planet Mars: From antiquity to the present. In *Mars* (H. H. Kieffer et al., eds.), pp. 1–33. Univ. of Arizona, Tucson.

Leinhardt Z. M., Richardson D. C., and Quinn T. (2000) Direct N-body simulations of rubble pile collision. *Icarus, 146,* 133–151.

Leinhardt Z. M. and Richardson D. C. (2002) N-body simulations of planetesimal evolution: Effect of varying impactor mass ratio. *Icarus,* in press.

Love S. G. and Ahrens T. J. (1996) Catastrophic impacts on gravity dominated asteroids. *Icarus, 124,* 141–151.

Love S. G., Horz F., and Brownlee D. E. (1993) Target porosity effects on impact cratering, and collisional disruption. *Icarus, 105,* 215–224.

McKinnon W. B. and Schenk P. M. (1995) Estimates of comet fragment masses from impact crater chains. *Geophys. Res. Lett., 22,* 1829–1832.

Melosh H. J. and Ryan E. V. (1997) Asteroids: Shattered but not dispersed. *Icarus, 129,* 562–564.

Melosh H. J. and Schenk P. (1993) Split comets and the origin of crater chains on Ganymede and Callisto. *Nature, 365,* 731–733.

Melosh H. J. and Stansberry J. A. (1991) Doublet craters and the tidal disruption of binary asteroids. *Icarus, 94,* 171–179.

Melosh H. J. and Whitaker E. A. (1994) Lunar crater chains. *Nature, 369,* 713–714.

Merline W. J., Close L. M., Dumas C., Chapman C. R., Roddier F., Menard F., Slater D. C., Duvert G., Shelton C., and Morgan T. (1999) Discovery of a moon orbiting the asteroid 45 Eugenia. *Nature, 401,* 565–568.

Merline W. J., Close L. M., Dumas C., Shelton J. C., Menard F., Chapman C. R., and Slater D. C. (2000) Discovery of companions to asteroids 762 Pulcova and 90 Antiope by direct imaging. *Bull. Am. Astron. Soc., 32,* 1017.

Merline W. J., Weidenschilling S. J., Durda D. D., Margot J. L., Pravec P., and Storrs A. D. (2002) Asteroids *do* have satellites. In *Asteroids III* (W. F. Bottke Jr. et al., eds.), this volume. Univ. of Arizona, Tucson.

Michel P., Benz W., Tanga P., and Richardson D. C. (2001) Collisions and gravitational reaccumulation: Forming asteroid families and satellites. *Science, 294,* 1696–1700.

Mitchell D. L., Ostro S. J., Rosema K. D., Hudson R. S., Campbell D. B., Chandler J. F., and Shapiro I. I. (1995) Radar observations of asteroids 7 Iris, 9 Metis, 12 Victoria, 216 Kleopatra, and 645 Zelinda. *Icarus, 118,* 105–131.

Mottola S. and Lahulla F. (2000) Mutual eclipse events in asteroidal binary system 1996 FG3: Observations and a numerical model. *Icarus, 146,* 556–567.

Mottola S. and 15 colleagues (1995) The slow rotation of 253 Mathilde. *Planet. Space Sci., 43,* 1609–1913.

Murchie S. and Erard S. (1996) Spectral properties and heterogeneity of Phobos from measurements by Phobos 2. *Icarus, 123,* 63–86.

Ocampo A. C. and Pope K. O. (1996) Shuttle imaging radar (SIR-C) images reveal multiple impact craters at Aorounga, northern Chad (abstract). In *Lunar and Planetary Science XXVII,* pp. 977–978. Lunar and Planetary Institute, Houston.

Öpik E. J. (1950) Roche's limit: Rings of Saturn. *Irish Astron. J., 1,* 25–26.

Ostro S. J. (1993) Planetary radar astronomy. *Rev. Mod. Phys., 65,* 1235–1279.

Ostro S. J., Chandler J. F., Hine A. A., Rosema K. D., Shapiro I. I., and Yeomans D. K. (1990) Radar images of asteroid 1989 PB. *Science, 248,* 1523–1528.

Ostro S. J. and 11 colleagues (1995) Extreme elongation of asteroid 1620 Geographos from radar images. *Nature, 375,* 474–477.

Ostro S. J. and 15 colleagues (1999) Asteroid 4179 Toutatis: 1996 radar observations. *Icarus, 137,* 122–139.

Ostro S. J., Hudson R. S., Nolan M. C., Margot J., Scheeres D. J., Campbell D. B., Magri C., Giorgini J. D., and Yeomans D. K. (2000) Radar observations of asteroid 216 Kleopatra. *Science, 288,* 836–839.

Ostro S. J., Hudson R. S., Benner L. A. M., Giorgini J. D., Magri C., Margot J.-L., and Nolan M. C. (2002) Asteroid radar astronomy. In *Asteroids III* (W. F. Bottke Jr. et al., eds.), this volume. Univ. of Arizona, Tucson.

Pravec P. and Hahn G. (1997) Two-period lightcurve of 1994 AW1: Indication of a binary asteroid? *Icarus, 127,* 431–440.

Pravec P. and Harris A. W. (2000) Fast and slow rotation of asteroids. *Icarus, 148,* 12–20.

Pravec P., Wolf M., and Šarounová L. (1998) Occultation/eclipse events on binary asteroid 1991 VH. *Icarus, 133,* 79–88.

Pravec P., Harris A. W., and Michałowski T. (2002) Asteroid rotations. In *Asteroids III* (W. F. Bottke Jr. et al., eds.), this volume. Univ. of Arizona, Tucson.

Rampino M. R. and Volk T. (1996) Multiple impact event in the Paleozoic: Collision with a string of comets or asteroids? *Geophys. Res. Lett., 23,* 49–52.

Richardson D. C., Bottke W. F. Jr., and Love S. G. (1998) Tidal distortion and disruption of Earth crossing asteroids. *Icarus, 134,* 47–76.

Richardson D. C., Quinn T., Stadel J., and Lake G. (2000) Direct large-scale N-body simulations of planetesimal dynamics. *Icarus, 143,* 45–59.

Ryan E. V. and Melosh H. J. (1998) Impact fragmentation: From the laboratory to asteroids. *Icarus, 133,* 1–24.

Ryan E. V., Hartmann W. K., and Davis D. R. (1991) Impact experiments. 3. Catastrophic fragmentation of aggregate targets and relation to asteroids. *Icarus, 94,* 283–298.

Scheeres D. J., Ostro S. J., Werner R. A., Asphaug E., and Hudson R. S. (2000) Effects of gravitational interactions on asteroid spin states. *Icarus, 147,* 106–118.

Schenk P. M., Asphaug E., McKinnon W. B., Melosh H. J., and Weissman P. R. (1996) Cometary nuclei and tidal disruption: The geological record of crater chains on Callisto and Ganymede. *Icarus, 121,* 249–274.

Scott E. R. D., Haack H., and Love S. G. (2001) Formation of mesosiderites by fragmentation and reaccretion of a large differentiated asteroid. *Meteoritics & Planet. Sci., 36,* 869–891.

Scotti J. V. and Melosh H. J. (1993) Estimate of the size of comet Shoemaker-Levy 9 from a tidal breakup model. *Nature, 365,* 733–735.

Sekanina Z. (2000) Secondary fragmentation of the Solar and Heliospheric Observatory sungrazing comets at very large heliocentric distance. *Astrophys. J. Lett., 542,* L147–L150.

Sekanina Z. and Yeomans D. K. (1985) Orbital motion, nucleus precession, and splitting of periodic Comet Brooks 2. *Astron. J., 90,* 2335–2352.

Smith D. E., Lemoine F. G., and Zuber M. T. (1995) Simultaneous estimation of the masses of Mars, Phobos, and Deimos from spacecraft distant encounters. *Geophys. Res. Lett., 22,* 2171–2174.

Solem J. C. and Hills J. G. (1996) Shaping of Earth-crossing asteroids by tidal forces. *Astron. J., 111,* 1382–1387.

Spray J. G., Kelley S. P., and Rowley D. B. (1998) Evidence for a late Triassic multiple impact event on Earth. *Nature, 392,* 171–173.

Sridhar S. and Tremaine S. (1992) Tidal disruption of viscous bodies. *Icarus, 95,* 86–99.

Sullivan R. and 17 colleagues (1996) Geology of 243 Ida. *Icarus, 120,* 119–139.

Thomas P. C. (1999) Large craters on small objects: Occurrence, morphology, and effects. *Icarus, 142,* 89–96.

Thomas P. C., Veverka J., Bloom A., and Duxbury T. (1979) Grooves on Phobos: Their distribution, morphology, and possible origin. *J. Geophys. Res., 84,* 8457–8477.

Thomas P. C., Adinolfi D., Helfenstein P., Simonelli D., and Veverka J. (1996) The surface of Deimos: Contribution of materials and processes to its unique appearance. *Icarus, 123,* 536–556.

Thomas P. C. and 11 colleagues (1999) Mathilde: Size, shape, and geology. *Icarus, 140,* 17–27.

Veverka J. and T. C. Duxbury (1977) Viking observations of Phobos and Deimos: Preliminary results. *J. Geophys. Res., 82,* 4213–4223.

Veverka J., Thomas P., Simonelli D., Belton M. J. S., Carr M., Chapman C., Davies M. E., Greeley R., Greenberg R., and Head J. (1994) Discovery of grooves on Gaspra. *Icarus, 107,* 72–83.

Veverka J. and 16 colleagues (1997) NEAR's flyby of 253 Mathilde: Images of a C asteroid. *Science, 278,* 2109–2114.

Veverka J. and 13 colleagues (1999) NEAR encounter with asteroid 253 Mathilde: Overview. *Icarus, 140,* 3–16.

Veverka J. and 32 colleagues (2001) Imaging of small-scale features on 433 Eros from NEAR: Evidence for a complex regolith. *Science, 292,* 484–491.

Viateau B. (2000) Mass and density of asteroids (16) Psyche and (121) Hermione. *Astron. Astrophys., 354,* 725–731.

Ward W. R. (2000) On planetesimal formation: The role of collective particle behavior. In *Origin of the Earth and Moon* (R. M. Canup and K. Righter, eds.), pp. 75–84. Univ. of Arizona, Tucson.

Weaver H. A. and 20 colleagues (2001) HST and VLT investigations of the fragments of Comet C/1999 S4 (LINEAR). *Science, 292,* 1329–1333.

Weidenschilling S. J. (1980) Hektor: Nature and origin of a binary asteroid. *Icarus, 44,* 807–809.

Weidenschilling S. J. (1981) How fast can an asteroid spin? *Icarus, 46,* 124–136.

Weidenschilling S. J. (1994) Origin of cometary nuclei as "rubble piles." *Nature, 368,* 721–723.

Weidenschilling S. J. (1997) The origin of comets in the solar nebula: A unified model. *Icarus, 127,* 290–306.

Weidenschilling S. J. and Cuzzi J. N. (1993) Formation of planetesimals in the solar nebula. *Protostars and Planets III* (E. Levy and J. I. Lunine, eds.), pp. 1031–1060. Univ. of Arizona, Tucson.

Weissman P. R. (1980) Physical loss of long-period comets. *Astron. Astrophys., 85,* 191–196.

Weissman P. R. (1982) Terrestrial impact rates for long- and short-period comets. In *Geological Implications of Impacts of Large Asteroids and Comets on Earth* (L. T. Silver and P. H. Schultz, eds.), pp. 15–24. GSA Special Paper 190.

Weissman P. R. (1986) Are cometary nuclei primordial rubble piles? *Nature, 320,* 242–244.

Wichman R. W. and Wood C. A. (1995) The Davy crater chain: Implications for tidal disruption in the Earth-Moon system and elsewhere. *Geophys. Res. Lett., 22,* 583–586.

Wilson L., Keil K., and Love S. J. (1999) The internal structures and densities of asteroids. *Meteoritics & Planet. Sci., 34,* 479–483.

Yeomans D. K. and 12 colleagues (1997) Estimating the mass of asteroid 253 Mathilde from tracking data during the NEAR flyby. *Science, 278,* 2106–2109.

Yeomans D. K. and 15 colleagues (2000) Radio science results during the NEAR-Shoemaker spacecraft rendezvous with Eros. *Science, 289,* 2085–2088.

Zuber M. T. and 11 colleagues (2000) The shape of 433 Eros from the NEAR-Shoemaker laser rangefinder. *Science, 289,* 2097–2101.